Nanoscale Res Lett (2010) 5:389–397
DOI 10.1007/s11671-009-9494-4

NANO EXPRESS

Self Assembly and Properties of C:WO_3 Nano-Platelets and C:VO_2/V_2O_5 Triangular Capsules Produced by Laser Solution Photolysis

B. W. Mwakikunga · A. Forbes · E. Sideras-Haddad · M. Scriba · E. Manikandan

Received: 24 October 2009 / Accepted: 11 November 2009 / Published online: 1 December 2009

Abstract Laser photolysis of WCl_6 in ethanol and a specific mixture of V_2O_5 and VCl_3 in ethanol lead to carbon modified vanadium and tungsten oxides with interesting properties. The presence of graphene's aromatic rings (from the vibrational frequency of 1,600 cm^{-1}) together with C–C bonding of carbon (from the Raman shift of 1,124 cm^{-1}) present unique optical, vibrational, electronic and structural properties of the intended tungsten trioxide and vanadium dioxide materials. The morphology of these samples shows nano-platelets in WO_x samples and, in VO_x samples, encapsulated spherical quantum dots in conjunction with fullerenes of VO_x. Conductivity studies revealed that the VO_2/V_2O_5 nanostructures are more sensitive to Cl than to the presence of ethanol, whereas the C:WO_3 nano-platelets are more sensitive to ethanol than atomic C.

Keywords Carbon · VO_2 · V_2O_5 · WO_3 · Laser · Photolysis · Sensors

B. W. Mwakikunga (✉) · A. Forbes
CSIR National Laser Centre, P. O. Box 395, Pretoria 0001, South Africa
e-mail: bmwakikunga@csir.co.za

A. Forbes
e-mail: aforbes1@csir.co.za

B. W. Mwakikunga · E. Sideras-Haddad
DST/NRF Centre of Excellence in Strong Materials and School of Physics, University of the Witwatersrand, Johannesburg, South Africa

B. W. Mwakikunga
Department of Physics, University of Malawi-The Polytechnic, Private Bag 303, Chichiri, Blantyre 3, Malawi

E. Sideras-Haddad
iThemba LABS, Private Bag 11, Wits 2050, Jan Smuts & Empire Rd., Johannesburg, South Africa

A. Forbes
School of Physics, University of Kwazulu-Natal, Private Bag X54001, Durban 4000, South Africa

M. Scriba · E. Manikandan
DST/CSIR National Centre for Nano-Structured Materials, P. O. Box 395, Pretoria, South Africa

Introduction

The study of vanadium and tungsten oxides has been undertaken extensively in recent years due to their respective thermo-chromic and electro-chromic and hence gas-chromatic properties. Since the discovery of the metal-to-insulator transition (MIT) at 340 K of VO_2 in 1959 by Morin [1] and electro-chromism of WO_3 in 1975 by Faughnan [2, 3], and also due to the fact that the tungsten metal is, so far, the best known dopant in VO_2 to reduce the MIT temperature to room temperature, the study of the two materials together is expected to yield a good understanding of their MIT behaviours especially at the nano-scale as discussed by this group and others previously [4–6]. To date, self assembly of these materials has been achieved by a number of techniques, including: hydrothermal techniques [7], employing templates either with polymers or pre-assembled carbon nanotubes [8], CVD epitaxial growth [9], sol–gel [10], ion implantation [11], hot-wire CVD [12], sputtering [13] and ultrasonic spray pyrolysis [14–18]. Also V_2O_5 capsules [19], WO_3 nano-rods and nano-wires and nano-arrays [20–22] have previously been obtained using several techniques. Laser synthesis methods have been of particular interest and have been followed by this group previously [23, 24]. The

coherent, intense and almost monochromatic laser light allows it to be tuned to selectively dissociate specific bonds in a precursor molecule either by resonance between the laser frequency and the bond's natural frequency or via multi-photon absorption. This leads to products that can be unique and different from those obtained by traditional thermal deposition techniques. In this work, we followed a process called laser solution photolysis (LSP) that has been used previously to obtain FePt ultra-fine powders [25]. Organo-metallic precursors containing Fe and Pt, respectively were employed in the presence of a polymer. The polymer was employed to reduce agglomeration of the nano-particles produced. Further examples of the technique include, gold nanoparticles produced by UV light irradiation of gold chloride [26–28], iron-based nanoparticles produced by utilising UV light absorbing ferrocene and iron(II) acetylacetonate [29, 30] and laser ablation in a solid–liquid interface [31, 32]. In this study, we used, as precursors, metal ethoxides which were produced from metal chlorides.

Experimental

During the preparation of the tungsten-based precursor solution, a complicated set of reactions take place over several days. This is indicated by the many continuous changes in the colour of the mixture of WCl_6 and ethanol. In accordance with the formation of vanadium ethoxide reported previously by Livage et al. [33], the possible reaction path for the dissolution of WCl_6 in ethanol is:

$$\begin{aligned} &WCl_6(\text{darkblue}) + C_2H_5OH \\ &\rightarrow \begin{cases} \mapsto WCl_5OR + HCl(\text{bluish\_green}) \\ \quad\quad\downarrow\uparrow \\ \quad WCl_4(OR)_2 + HCl \\ \downarrow\uparrow (\text{greenish\_yellow}) \\ \quad\quad\vdots \\ W(OR)_6\,(\text{light\_yellow}) \end{cases} \end{aligned} \quad (1)$$

Most of the HCl is lost as gas bubbles, which visibly effervesce from the liquid. Similar reaction routes are expected for the vanadium dioxide precursor solution.

For the synthesis of WO_3, an aliquot of 5.3 mg of a dark-blue WCl_6 powder was dissolved in 500 ml of ethanol in an argon environment, resulting in a light blue to light-yellow liquid. When this liquid was irradiated with 5,000 saw-tooth-shaped pulses from a 248-nm KrF excimer laser, with a fixed energy of 10 mJ at 8 Hz, the light yellow liquid turned to blue-black. For the production of VO_2, one part of V_2O_5 (in which molecule the V takes the valence of 5+) and two parts of VCl_3 (where V has a valence of 3+) were dissolved in ethanol. The ratio was chosen to produce a stoichiometry of VO_2 in which molecule the V atom has a valence of 4+.

Scanning electron microscopy was carried on a Gemini Neon 40 FEG SEM equipped with a focussed ion beam (FIB) gun. A drop of the as-irradiated liquid was dropped onto a glass slide and Si(111) surface. Raman spectroscopy was carried out using a Jobin–Yvon T64000 Raman spectrograph with a 514.5-nm line from an argon ion laser. The power of the laser at the post-annealed samples (0.384 mW) was small enough in order to minimise localised heating of the sample. The T64000 was operated in single spectrograph mode, with the 1,800 lines/mm grating and a 50× objective on the microscope. A drop of such liquid was also placed on carbon holey film supported by copper grids for high resolution transmission electron microscopy on a JEOL 2100 equipped with a LaB_6 filament and a Gartan U1000 camera with 2,028 × 2,048 pixels.

Results and Discussion

When the tungsten ethoxide is irradiated with a 10.6-μm CO_2 laser beam, the O–C bond, whose vibrational frequency of 1,000 cm^{-1} is close to that of the laser (944 cm^{-1}), is selectively dissociated by multi-photon absorption to produce WO_3 via:

$$\begin{aligned} 2W(O-C_2H_5)_6 &\xrightarrow{10.6\,\mu m} 2WO_{3-x}(\text{yellow}) \\ &\quad + (12-y)C + (15-z)H_2 \\ 2V(O-C_2H_5)_4 &\xrightarrow{10.6\,\mu m} 2VO_{2-x}(\text{yellowish brown}) \\ &\quad + (12-y)C + (15-z)H_2 \end{aligned} \quad (2)$$

The laser dissociation route in Eq. 2 was reported previously when non-stoichiometric WO_3 thin films [23] were observed in laser pyrolysed samples by Raman spectroscopy. The films became stoichiometric WO_3 nanowires after further post-deposition annealing in a furnace [24]. In the same sample, isolated carbon material such as multi-wall carbon nano-tubes were seen under TEM. It is presumed that the H_2 evaporated during the laser pyrolysis and annealing. Furthermore, as shown in Eq. 2, carbon is segregated and deposits as one or more of its allotropes such as tetrahedrally amorphous carbon, graphite and diamond. However, carbon can also be found in the matrix of WO_3 as a dopant as in Eq. 3. This has been observed in the current set of experiments.

$$2W(O-C_2H_5)_6 \xrightarrow{248nm} C_xWO_{3-y} + \ldots$$
$$2V(O-C_2H_5)_4 \xrightarrow{248nm} C_xVO_{2+y} + \ldots \quad (3)$$

When the same precursors are irradiated with the 248-nm beam from the KrF excimer laser, the $W(OR)_6$ liquid turns blue-black before stabilising to a yellow colour after a few days, whereas no colour change is seen in the vanadium precursor. It is suggested that at this wavelength, a different bond is dissociated namely the C–H bond which has a frequency of between 3,000 and 3,300 cm^{-1} compared to the laser frequency of 40,322 cm^{-1} (at $\lambda =$ 248 nm). The C–H bond then has a higher probability of being dissociated than the O–C bond, since the C–H bond is only 10 times lower than the laser frequency when compared to the O–C which is 40 times lower. Also, the C–H bond is capable of oscillating closer to the laser frequency via other higher order vibrational modes.

The scanning electron microscopy image of carbon modified WO_x nano-platelets presented in Fig. 1 shows significant stacking between the platelets and the formation of chains. A relatively narrow size distribution of the particles can be observed. Local EDS (inset of Fig. 1) demonstrates the purity of the carbon modified WO_3 sample. A carbon shoulder peak at X-ray energy of about 0.3 keV could clearly be observed.

X-ray diffraction (XRD) results from the carbon modified WO_3 nano-platelets are presented in Fig. 2. In our carbon modified WO_3 sample, the usual triplet peaks at 2θ values of 23.117°, 23.583° and 24.583° corresponding to the Miller indices of (002), (020) and (200) (International

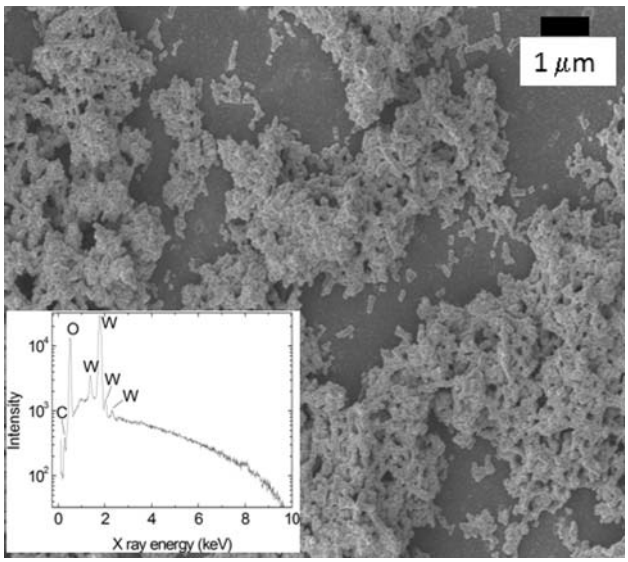

Fig. 1 Scanning electron micrograph of the carbon modified WO_3 particles produced by laser solution photolysis. The inset shows elemental composition of the sample by EDS

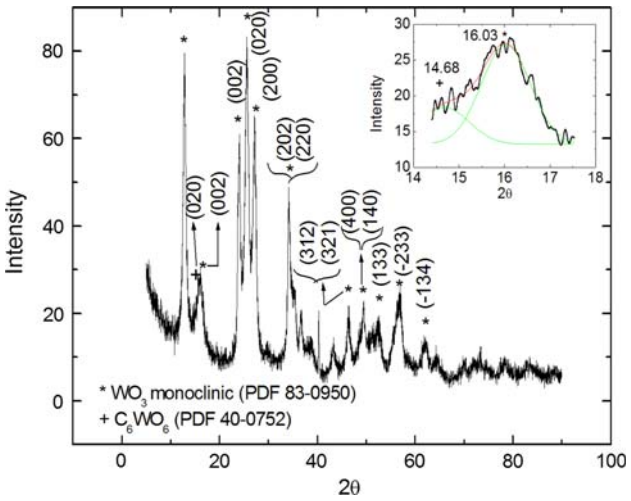

Fig. 2 X-ray diffraction of the carbon modified WO_3 nano-platelets. Note the shoulder peak at $2\theta = 14.63°$ which closely matches that of C_6WO_6 at $2\theta = 15.595°$

Crystallographic Diffraction Data (ICDD) Powder Diffraction File (PDF) 83-0950) are found to be shifted to $2\theta = 23.736°$, 25.463° and 27.325°, respectively. This indicates that this is indeed the WO_3 crystal but its structure is significantly distorted by dopants. Based on the initial reagents and EDS spectrum in the inset of Fig. 1, the dopant for WO_3 nanoplates is only carbon. No hydrogen or chlorine peaks were found. From more searches in the ICDD database, the PDF No 40-0752 of C_6WO_6 has a strong peak at $2\theta = 15.595°$ with the (*hkl*) coordinates of (002) or (101) which closely matches the shoulder peak in the present sample at $2\theta = (14.63 \pm 0.54)°$. This peak is not found in all files of stoichiometric WO_3. This suggests that carbon is the most important dopant in this case.

The distortion of the WO_3 structure observed by high resolution transmission electron microscopy (Fig. 3) supports the XRD results. The (002), (020) and (200) planes in stoichiometric WO_3 (PDF 80-0950) are expected to have *d*-spacings of 3.8443, 3.7694 and 3.6499 Å. Based on the TEM observations of our carbon modified WO_3 crystals, the inter-planar *d*-spacings are 4.70, 3.52 and 3.38 Å, respectively.

Our VO_x sample was also prepared similarly and observed by TEM. Triangular envelope-like structures of about 400 nm on each side of the triangle are the predominant polymorphs. The triangles are thin layers of VO_x with an interplanar spacing of 3.75 Å as shown in Fig. 4. Observed at higher magnification, the layers were found to be envelopes containing spherical nano-particles with an average size of 6 nm. These VO_x quantum dots which can be solid (multi-walled) spheres or VO_x fullerenes are found to have the same size distribution, as shown in the inset (d) of Fig. 4. An EDS spectrum of such nanostructures placed

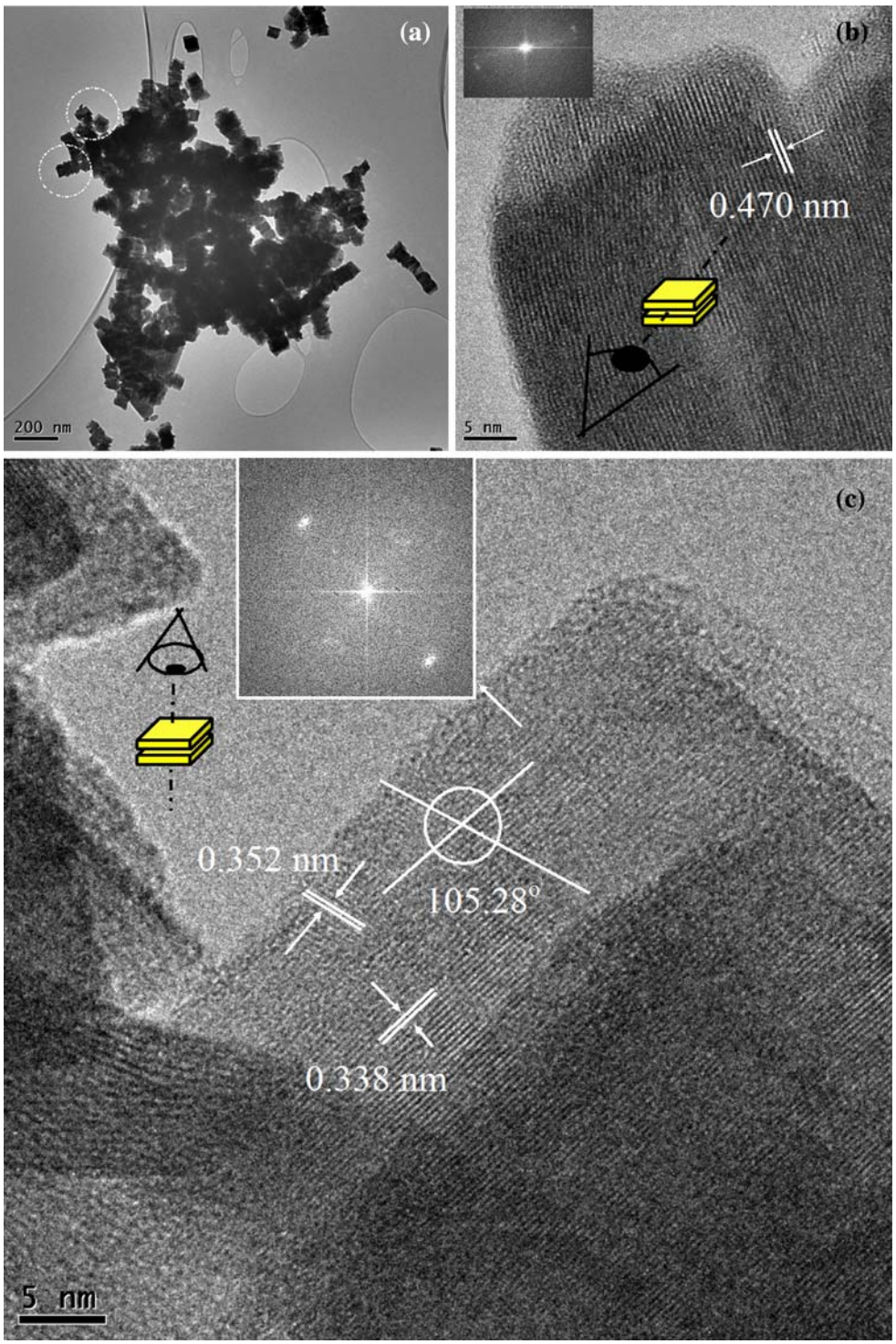

Fig. 3 **a** Low magnification TEM image of the WO_x showing stacking of nano-platelets, **b** cross-sectional view of one stacking, showing each platelet can be up to 20 nm thick with one preferred direction of stacking as shown by the inset of the image's FFT. **c** Top-view of two platelets stacked together showing the inter-planar spacing, angles and the two-dimensional growth shown by FFT of the image in the inset of **c**

on Si(111) surface (inset (e) in Fig. 4) showed peaks for V and O alongside the major Si(111) from the substrate and trace amounts of Na, Cl and Ca. This confirms the morphology studies done by SEM of such a sample (not shown here) where the triangular capsules were interspaced by large cubic crystals presumably of NaCl and $CaCl_2$ which have been segregated from the V_2O_5/VO_2 triangular capsules. Also, carbon doping is confirmed in the capsules by the C shoulder peak at 0.3 keV.

From Raman spectroscopy of the carbon modified WO_x shown in Fig. 5, a slight red-shift from 705 to 674 cm^{-1} can be observed, corresponding to the bending modes in WO_3 of O–W–O. The suppression of the stretching mode of the same bond at 800 cm^{-1} is presumed to be due to the

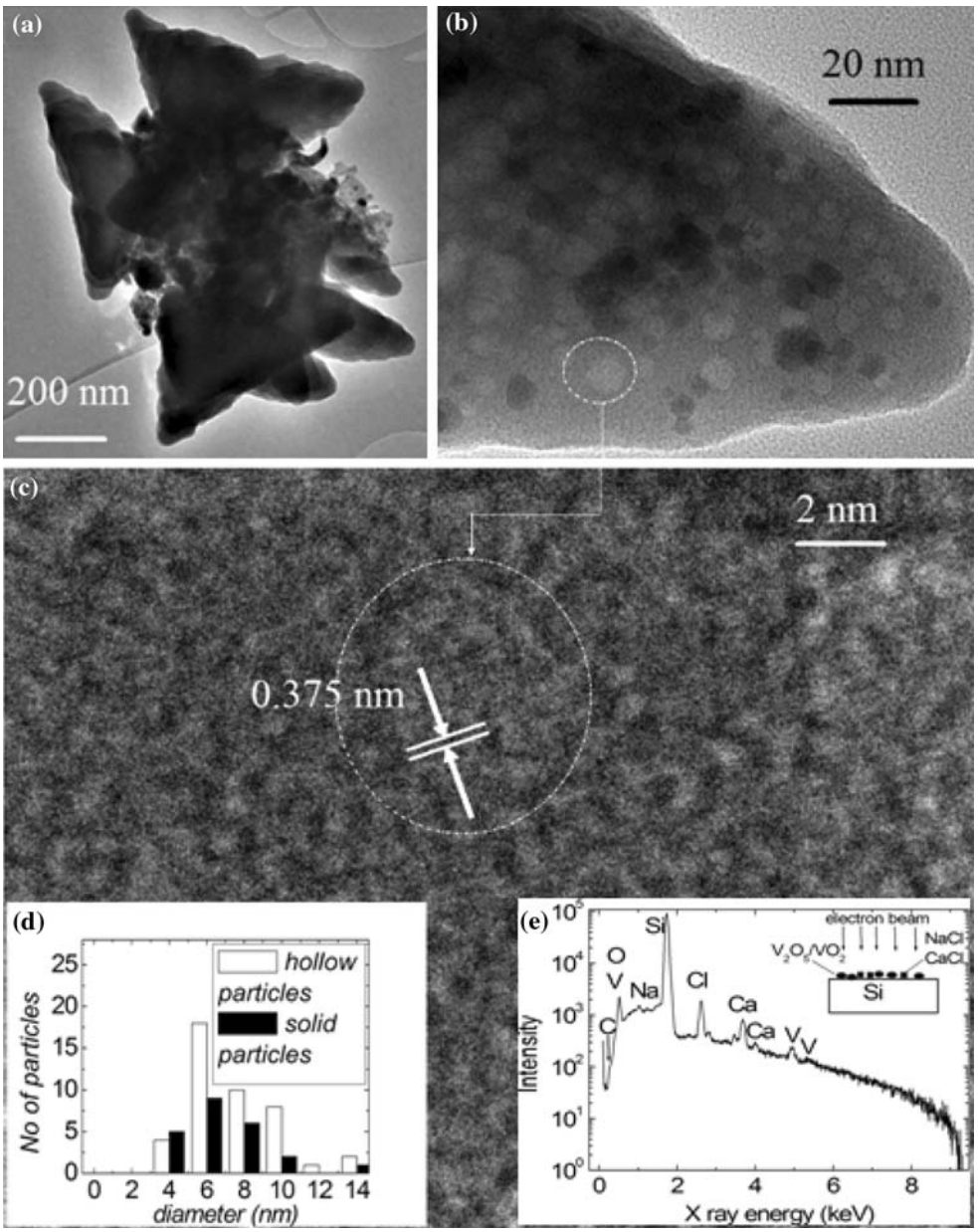

Fig. 4 **a** Low magnification TEM of the triangular envelopes of VO_x, **b** one pocket at higher magnification, showing the small voids and solid spheres, **c** HRTEM of one of the hollow quantum dots and, **d** size distribution histograms for the hollow and solid quantum dots of VO_x and **e** EDS of the C: V_2O_5/VO_2 nanostructures showing their elemental composition

presence of the dopants. Only the surface W=O stretching mode at 958 cm^{-1} is unchanged by the new structure. This peak is broadened towards the higher wave-numbers—beyond 1,000 cm^{-1}. It should also be noted that the O–C bond found in ethanol, which could be the bridge between the dopant carbon and the WO_6 octahedra in the WO_3 structure in this case, has a vibrational frequency of 1,000 cm^{-1} [34]. The presence of carbon is signified by the peak close to 1,580 cm^{-1} showing aromatic rings of carbon which form the perfect graphite sp^2 bonding structure. We did not find any D band at 1,354 cm^{-1} in this sample showing that there is no disorder in the aromatic network structure of the dopant C. However, there is a new sharp peak at 1,124 cm^{-1} which could be assigned to C–C bond vibration, in agreement with previously observed glucose carbon vibrations at 1,126 cm^{-1} [34]. Ferrari et al. [35] previously observed a peak at 1,060 cm^{-1} in diamond-like-carbon and assigned this phonon frequency to sp^3 bonding but this was found to be too far from the 1,124 cm^{-1} peak observed presently to be acceptable.

Fourier-transform infrared spectroscopy of the carbon modified WO_3 (Fig. 6) supports the results obtained by

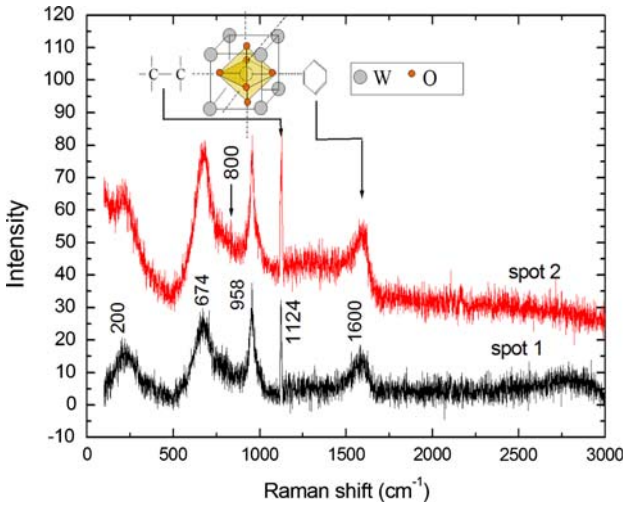

Fig. 5 Raman spectra of the carbon modified WO_x nano-platelets showing the characteristics peaks for the crystal WO_3 and those of aromatic carbon at 1,600 cm^{-1}. The peak at 1,124 cm^{-1} closely matches that of 1,126 cm^{-1} assigned to C–C bond vibration

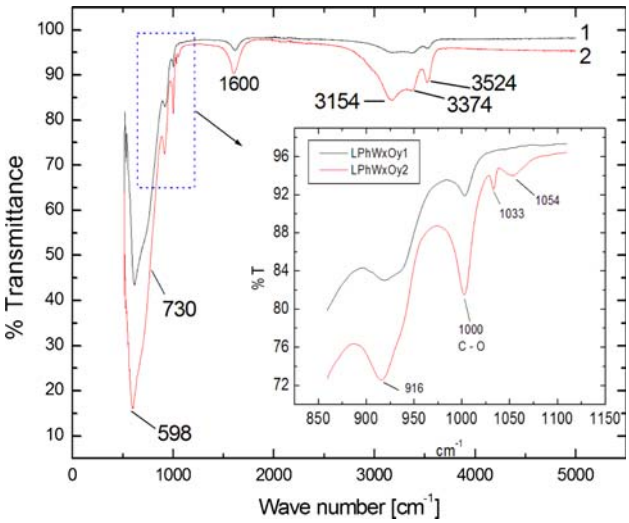

Fig. 6 Infrared spectra of two samples of carbon-doped WO_3. Sample 2 was exposed to carbon for a longer period of time than sample 1. The carbon doping is confirmed by the existence of the carbon–oxygen bond at 1,000 and 1,054 cm^{-1} in both samples

Raman spectroscopy. The strong and broad absorption peak at 598 cm^{-1} with its shoulder at 730 cm^{-1} can be assigned to the O–W–O stretching vibrations in the WO_3 structure, whereas the 916 cm^{-1} peak corresponds to the W=O surface stretching modes due to dangling oxygen bonds. The red-shift from the Raman allowed 960 cm^{-1} to the IR allowed 916 cm^{-1} could be due to the loading of carbon on these bonds. Carbon doping is confirmed by the presence of the peaks assigned to the C–O bonding at 1,000 and 1,054 cm^{-1}; these could not be observed in Raman spectroscopy for reasons not established yet. The 1,600 cm^{-1} phonon frequency assigned to the perfect graphite's aromatic carbon ring is confirmed by FTIR as previously seen in Raman spectroscopy. The group of absorption peaks from 3,000 to 3,550 cm^{-1} have previously been assigned to OH bonds which suggest that some terminal oxygen atoms in the WO_3 structure are not only bonded to the carbon aromatic rings but also to hydrogen. No C–H bonds were found by FTIR.

Possible Mechanism of Formation of the Triangular Envelopes and VO_x Inorganic Fullerenes

Since the discovery of carbon nano-tube structure in the early 1980s, Tenne and co-workers also reported similar structures in WSe_2 and MoS_2 [36]. The argument was that metal chalcogenides and oxides are also capable of arranging their unit cells in a hexagonal close packing as in carbon, thereby forming a layer of atoms whose edges leave dangling bonds. These bonds cause intense attractive forces which compel the layer to fold on itself into various shapes such as tubes, scrolls and rods. Formation of fullerenes is due to defects which are found to be pentagonal, rectangular and triangular bonds, which are possible in all transition metal compounds. Different processes of formation of, for instance, V_2O_5 capsules [37, 38] have led authors to suggest various mechanisms. We suggest that the formation of our triangular envelopes/capsules starts with the formation of closely packed hexagonal 2-D layers when the VO_x is subjected to the laser beam. This assumption is based on the known experimental and theoretical facts from computer modelling that V_2O_5 is capable of wrapping into V_2O_5 nano-tubes [39] either as a zig–zag framework or in an arm chair structure [40]. It is also known that a mixture of V^{4+} and V^{5+} in $(V^{IV}O)[V^{V}O_4].0.5[C_3N_2H_{12}]$ can lead to a layered structure [41]. The organic layer intercalates the inorganic counterpart with the latter containing square pyramids formed by V^{4+} ions and tetrahedral pyramids formed by V^{5+} ions. On this layer are randomly scattered fullerenes of the same material which have self-assembled under the same laser beam. These fullerenes together with dangling bonds on the layer periphery exert intense attractive forces which cause the layer to fold on itself in a certain pattern. A schematic cartoon of the possible formation of the VO_2/V_2O_5 triangular envelops that encapsulate the VO_2/V_2O_5 QDs and the VO_2/V_2O_5 fullerenes are shown in Fig. 7. A hexagonal packing in a zig–zag fashion ends up having arm-chair structure dangling bonds in the periphery of the hexagon. The dangling bonds and the van der Waal's forces from the particles sitting on the surface compel this sheeting to wrap

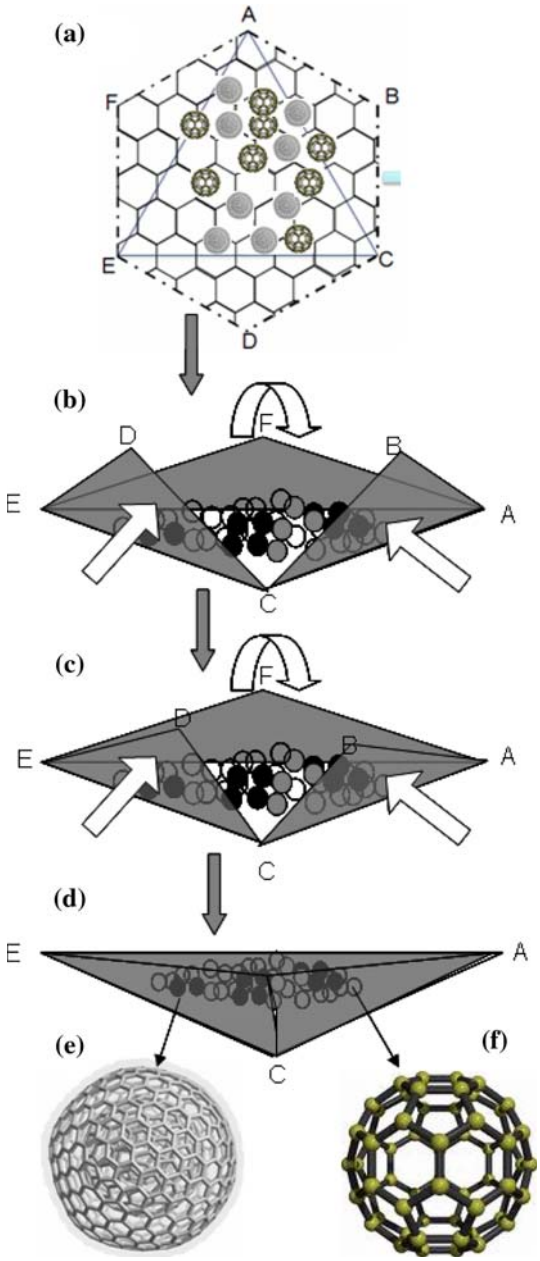

Fig. 7 A schematic representation of how the triangular envelops of VO_x sheets form **a** a hexagonally packed layer of V_2O_5/VO2 with some QDs of same material scattered randomly on it **b** the layer folds along zigzag AE, armchair EC and armchair AC of triangle AEC **c** the folding of triangular flaps ABC, CDE and EDF progresses until **d** the triangular envelop AEC is formed. The enveloped spherical particles are either **e** multi-walled V_2O_5/VO_2 fullerenes or **f** single walled V_2O_5/VO_2 fullerenes

on itself from a hexagon, through intermediate stages, into a triangular envelope. The foldings are along arm-chair structure on two sides of the triangle AEC (sides AC and EC in Fig. 7 (a)) and along a zig–zag structure on the third side of the triangle (side AE).

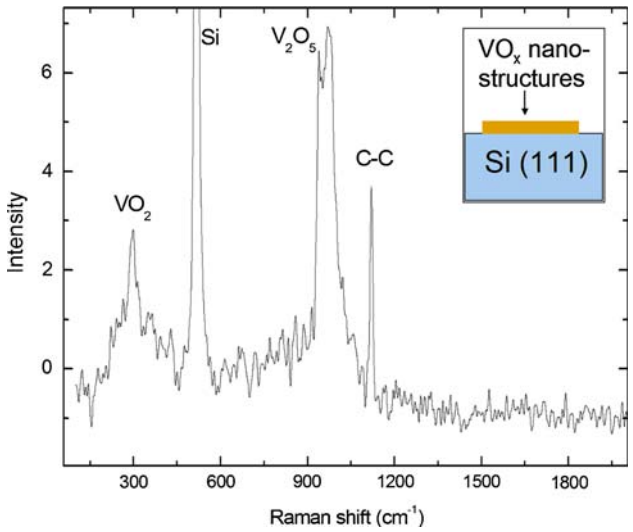

Fig. 8 Raman spectrum of the VO_2/V_2O_5 triangular capsules containing VO_2/V_2O_5 fullerenes and quantum dots showing a strong peak at 1,120 cm^{-1} which suggests C–C intercalation of the VO_2/V_2O_5 structure

Raman spectroscopy of these structures (shown in Fig. 8) supports the fact that there exists mixed valence of V^{4+} (signified by the 300 cm^{-1} phonon which is an undertone of the main 600 cm^{-1} peak which in these samples is masked by the strong Si–Si background noise from the substrate at 520 cm^{-1}) and V^{5+} from 930–970 cm^{-1}. The peak at 1,120 cm^{-1} suggests the presence of C–C bonds in the VO_2/V_2O_5 structure. As opposed to the carbon modified WO_3 nano-platelets which showed aromatic carbon apart from C–C bonds, Raman spectroscopy showed no aromatic rings in VO_2/V_2O_5 triangular envelopes.

Influence of Chlorine on the Conductance of VO_x Structures

Two samples of the VO_2/V_2O_5 triangular envelopes were produced from laser photolysis of VCl_3 in ethanol and V_2O_5 added to VCl_3 in ethanol were subjected to conductivity tests using a four-point probe technique by employing a Keithley Semiconductor Characterisation System (Fig. 9). Pure V_2O_5 powder shows negligible conductance (inset of Fig. 9) which is enhanced by performing laser photolysis in the presence of VCl_3 in ethanol. The conductance is highest in the photolysed VO_2/V_2O_5 nanostructures produced from the precursor of VCl_3 in ethanol. This suggests that in the first photolysis, we form VO_x nanostructures of lower content of Cl than in the second one. Furthermore, the VO_x structures are sensitive to the presence of Cl which could indicate that VO_x

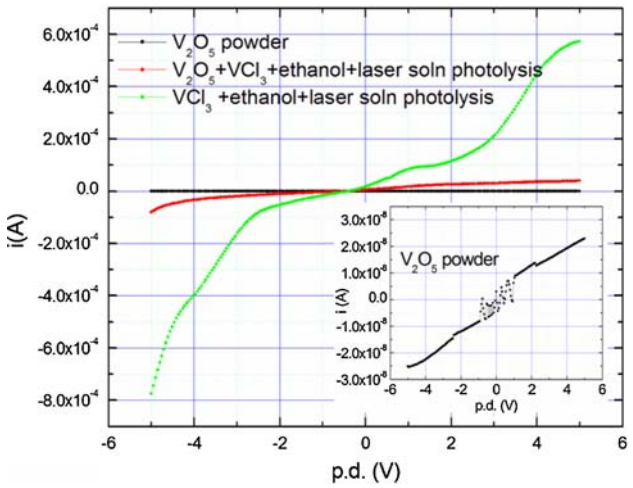

Fig. 9 The high conductance in photolysed VCl_3 in ethanol shows the higher sensitivity of VO_2/V_2O_5 triangular envelopes to chlorine exposure compared to ethanol. Inset: the i-v curve for pure V_2O_5 powder

nanostructures are potential chlorine sensors. In both samples, the presence of chlorine shows a more pronounced change than the presence of ethanol.

Effect of Ethanol on the Conductance of WO_x Platelets

Two C:WO_3 samples produced by laser solution photolysis were dried for two and 3 weeks respectively. The sample dried for 3 weeks was assumed to be more heavily carbon-doped and it only showed slightly more conductivity than the sample dried for 2 weeks as shown in the inset of Fig. 10. However, exposure of these C:WO_3 nano-platelets to ethanol significantly increased the conductance, confirming that WO_3 can act as a sensor of ethanol.

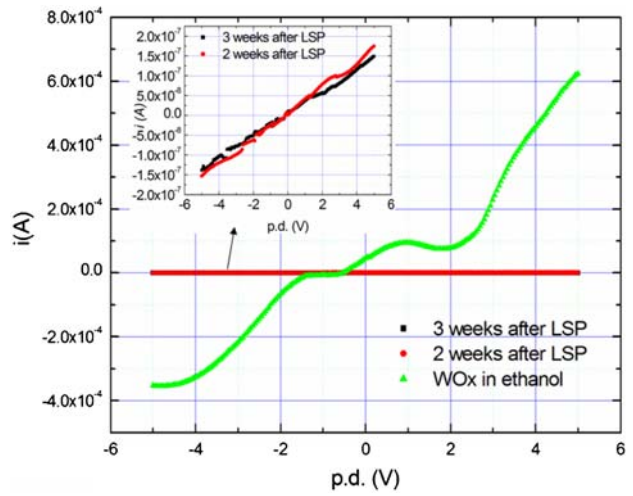

Fig. 10 The presence of ethanol in the C:WO_3 nano-platelets shows a more pronounced change in conductivity than the presence of carbon

Conclusion

Production of nano-platelets of carbon modified WO_3 and 6-nm encapsulated VO_x quantum dots by laser solution photolysis have been achieved. Conductivity studies revealed that the VO_2/V_2O_5 nanostructures are more sensitive to atomic C than to the presence of ethanol, whereas the C:WO_3 nano-platelets are more sensitive to ethanol than atomic C.

Acknowledgments We acknowledge Nosipho Moloto for her assistance with FIB FEGSEM, Brian Yalisi for the KrF laser and Lerato Shikwambana and Malcolm Govender for the starting materials. Financial and infrastructural support from the CSIR National Laser Centre and characterisation facilitation of the CSIR National Centre for Nano-Structured Materials are acknowledged.

References

1. F.J. Morin, Phys. Rev. Lett. **3**, 34 (1959)
2. B.W. Faughnan, R.S. Crandall, P.M. Heyman, R.C.A. Review **36**, 177 (1975)
3. B.W. Faughnan, R.S. Crandall, M.A. Lampert, Appl. Phys. Lett. **27**, 275 (1975)
4. C.G. Granqvist, A. Azens, A. Hjelm, L. Kullman, G.A. Niklasson, D. Rönnow, M. Strømme Mattsson, M. Veszelei, G. Vaivars, Sol. Energy **63**, 199–216 (1998)
5. B.W. Mwakikunga, E. Sideras-Haddad, A. Forbes, S.S. Ray, C. Arendse, G. Katumba, in *Metal–to–insulator transitions and the thermochromism of VO_2 at nanoscale in chromic materials, phenomena and their applications*, ed. by P. Somani (Applied Science Innovations Private Limited (ASIPL), Maharashtra, India, 2009)
6. F. Sediri, N. Gharbi, J. Phys. Chem. Solids **68**, 1821 (2007)
7. B. Li, X. Ni, F. Zhou, J. Cheng, H. Zheng, M. Ji, Solid State Sci. **8**, 1168 (2006)
8. X.-W. Chen, Z. Zhu, M. Havecker, D.S. Su, R. Schlogl, Mater. Res. Bull. **42**, 354 (2007)
9. P. Tägtström, U. Jansson, Thin Solid Films **352**, 107 (1999)
10. J. Yan, W. Huang, Y. Zhang, X. Liu, M. Tu, Physica Status Solidi (A) Appl. Mater. **205**(10), 2409–2412 (2008)
11. L.A. Gea, L.A. Boatner, Appl. Phys. Lett. **68**(22), 3081–3083 (1996)
12. A.H. Mahan, P.A. Parilla, K.M. Jones, A.C. Dillon, Chem. Phys. Lett. **413**, 88 (2005)
13. T. Ben-Messaoud, G. Landry, J.P. Gariépy, B. Ramamoorthy, P.V. Ashrit, A. Haché, Opt. Commun. **281**(24), 6024–6027 (2008)
14. B.W. Mwakikunga, E. Sideras-Haddad, M. Maaza, Optical Mater. **29**(5), 481 (2007)
15. B.W. Mwakikunga, E. Sideras-Haddad, M. Witcomb, C. Arendse, A. Forbes, J. Nanosci. Nanotechnol. **9**, 3286 (2008)
16. B.W. Mwakikunga, A. Forbes, E. Sideras-Haddad, C. Arendse, Phys. Stat. Solidi (a) **205**, 150 (2008)
17. B.W. Mwakikunga, E. Sideras-Haddad, C. Arendse, A. Forbes, OAtube Nanotechnol. **2**, 109 (2009) http://www.oatube.org/2009/01/ bwmwakikunga.html

18. B.W. Mwakikunga, E. Sideras-Haddad, C. Arendse, A. Forbes, P. C. Eklund, T. Malwela, T.K. Hillie, S. Sinha-Ray, Nano Lett (2009) (submitted)
19. J. Liu, H. Xia, D. Xue, L. Lu, J. Am. Chem. Soc. **131**, 12086 (2009)
20. S. Rajagopal, D. Nataraj, D. Mangalaraj, Y. Djaoued, J. Robichaud, O.Yu. Khyzhun, Nanoscale Res. Lett. **4**, 1335 (2009)
21. J. Rajeswari, P.S. Kishore, B. Viswanathan, T.K. Varadarajan, Nanoscale Res. Lett. **2**, 496 (2007)
22. X.P. Wang, B.Q. Yang, H.X. Zhang, P.X. Feng, Nanoscale Res. Lett. **2**, 405 (2007)
23. B.W. Mwakikunga, A. Forbes, E. Sideras-Haddad, R.M. Erasmus, G. Katumba, B. Masina, Int. J. Nanoparticles **1**, 3 (2008)
24. B.W. Mwakikunga, A. Forbes, E. Sideras-Haddad, C. Arendse, Nanoscale Res. Lett. **3**, 372 (2008)
25. M. Watanabe, H. Takamura, H. Sugai, Nanoscale Res. Lett. **4**, 565 (2009)
26. H. Hada, Y. Yonezawa, A. Yoshida, A. Kurakake, J. Phys. Chem. **80**, 2728 (1976)
27. K. Kurihara, J. Kizling, P. Stenius, J.H. Fendler, J. Am. Chem. Soc. **105**, 2574 (1983)
28. L. Bronstein, D. Chernshov, P. Valetsky, N. Tkachenko, H. Lemmetyinen, J. Hartmann, S. Forster, Langmuir **15**, 83 (1999)
29. J.A. Powell, S.R. Logan, J. Photochem. **3**, 189 (1974)
30. J. Pola, M. Marysko, V. Vorlicek, S. Bakardjieva, J. Subrt, Z. Bastl, A. Ouchi, J. Photochem. Photobiol. Chem. **199**, 156 (2008)
31. C. Liang, Y. Shimizu, M. Masuda, T. Sasaki, N. Koshizaki, Chem. Mater. **16**, 963 (2004)
32. Y. Ishikawa, K. Kawaguchi, Y. Shimizu, T. Sasaki, N. Koshizaki, Chem. Phys. Lett. **428**, 426 (2006)
33. J. Livage, Chem. Mater. **3**, 578 (1991)
34. A. Picard, I. Daniel, G. Montagnac, P. Oger, Extremophiles **11**, 445 (2007)
35. A.C. Ferrari, J. Robertson, Phys. Rev. B **64**, 075414 (2001)
36. R. Tenne, I. Margulis, M. Genut, G. Hodes, Nature **360**, 444 (1992)
37. J. Liu, D. Xue, Adv. Mater. **20**, 2622 (2008)
38. J. Liu, F. Liu, K. Gao, J. Wu, D. Xue, J. Mater. Chem. **19**, 6073 (2009)
39. G.T. Chandrappa, N. Stenou, S. Cassaignon, C. Bauvis, J. Livage, Catal. Today **78**, 85 (2003)
40. V.V. Ivanovskaya, A.N. Enyashin, A.A. Sofronov, Y.N. Makurin, N.I. Medvedeva, A.L. Ivanovskii, Solid State Commun. **126**, 489 (2003)
41. D. Riou, G. Ferey, J. Solid State Chem. **120**, 137 (1995)